Letters

A New PV System Configuration Based on Submodule Integrated Converters

Omair Khan, Weidong Xiao, and Mohamed Shawky El Moursi

***Abstract*—The power loss due to mismatch effect among interconnected photovoltaic (PV) modules can be significantly reduced by applying the maximum power point tracking to fine granularity level. In this paper, a novel configuration is proposed to utilize a submodule integrated converter (subMIC) for effective solar energy harvesting. Gallium Nitride (GaN) field-effect transistors (FETs) are used to construct the power circuits for high conversion efficiency and high power density. The detailed mathematical analysis is presented to provide insight into the architecture. Simulation is carried out to demonstrate the system behavior in response to real-world atmospheric conditions. The hardware prototype consisting of three subMICs is developed utilizing GaN FET as the power switches, which are based on industrial standard and are compact to fit into the junction box of commercial PV modules. The advantages in terms of conversion efficiency, system cost, and dynamic performance are experimentally proved by the comparison with a benchmark system.**

***Index Terms*—DC–DC power converters, energy harvesting, maximum power point tracking (MPPT), photovoltaic (PV) power systems.**

I. Introduction

PHOTOVOLTAIC (PV) power systems have been installed dramatically over years thanks to the technology improvement of PV materials and power electronics [1], [2]. In conventional PV power systems, the panels are arranged in series to achieve high stacked voltage at the dc link for grid connection. However, such configuration suffers significant power degradation in case of mismatch among connected PV modules. This can result from partial shading, dissimilar aging of PV panels, manufacturing imperfections, and dirt accumulation, etc. [3].

Distributed MPPT structures have been proposed to minimize the mismatch impact. The architectures of microinverter [4], differential power processor (DPP) [5], [6], submodule-level differential power processor (subDPP) [7]–[10], dc power optimizer (DCPO) [11], [12], and submodule integrated converters (subMICs) [13]–[16] have been introduced in literatures. The DCPOs and subMICs are categorized as full power processing (FPP) architectures because the distributed dc–dc converters process the entire power generated from the PV element. On the other hand, the systems of DPP and subDPP fall in the category of partial power processing architectures and process only the mismatch power. The subDPP and subMICs are controlled by maximum power point tracking (MPPT) on the submodule level in order to eliminate mismatches at finer granularity as compared to module-level MPPT solutions of DCPO and DPP. The submodule is a section of a PV panel, which is segmented into three or four subsections of 15 to 24 series-connected PV cells.

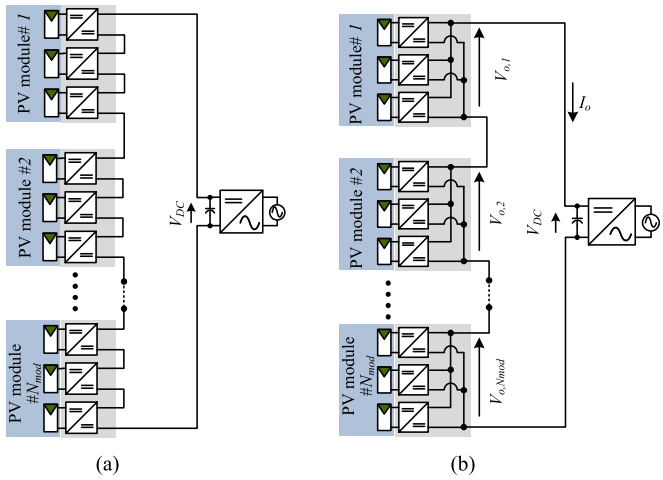

Fig. 1. (a) Conventional subMICs architecture. (b) Proposed PV power system architecture.

The cascaded subMICs have been shown to be effective in handling mismatches and providing efficient energy harvesting [13]. It shows the potential to be integrated inside the PV module junction box for easy installation and low cost. The inputs of converters are connected in parallel with PV submodules, while the converters are connected in series on the output terminal, as shown in Fig. 1(a). Consequently, converters share the same output current. The dc–dc converter topology with current step-up ability is recommended since the shaded submodules cannot generate the same current as the unshaded submodules. Therefore, the synchronous buck topology is preferred because of its ability to step-up the input current and has been utilized in [13]–[16] for subMIC implementation.

However, for PV applications, the boost converter topology is more suitable due to the low voltage nature of PV cells.

Manuscript received October 20, 2016; revised November 14, 2016; accepted November 27, 2016. Date of publication December 1, 2016; date of current version February 2, 2017.

O. Khan and W. Xiao are with the Department of Electrical Engineering and Computer Science, Masdar Institute, Abu Dhabi 54224, United Arab Emirates (e-mail: omairkhan.k@gmail.com; mwxiao@masdar.ac.ae).

M. S. E. Moursi is with the Department of Electrical Engineering and Computer Science, Masdar Institute, Abu Dhabi 54224, United Arab Emirates and is currently on leave from the Faculty of Engineering, Mansoura University, Mansoura 35516, Egypt (e-mail: melmoursi@masdar.ac.ae).

Color versions of one or more of the figures in this letter are available online at http://ieeexplore.ieee.org.

Digital Object Identifier 10.1109/TPEL.2016.2633564

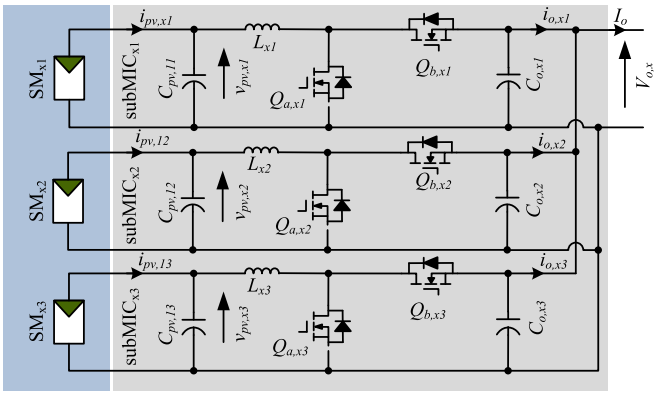

Fig. 2. Interconnection of submodules and subMICs in a single PV module.

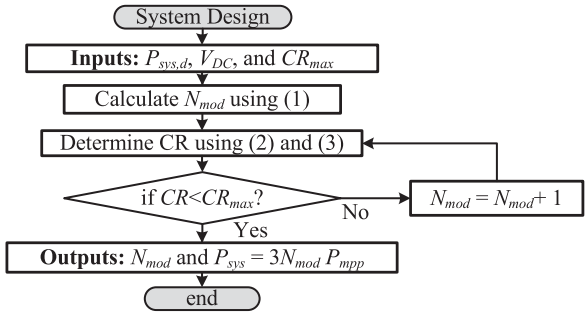

Fig. 3. Flowchart of the process to size the proposed PV power system.

One study created an equivalent environment to compare buck converter and boost converter used for PV side power interface [17] and evaluated the performance in terms of system dynamics and components cost. The results demonstrated the effectiveness of boost converter in terms of better dynamic performance and low-cost implementation. Therefore, to utilize the advantages of boost converter in distributed systems, a novel submodule-level PV power system architecture is proposed in this paper. The proposed solution aims at providing a simple and efficient solution for PV power extraction by utilizing synchronous boost converters.

In addition to the variation in terms of architectures, power transistor devices show significant impact on the performance of a PV system. The commonly used silicon-based MOSFET has already reached its theoretical limits [18]. Wide bandgap devices, such as silicon Carbide and Gallium Nitride have been utilized in power electronic applications [19] showing the advantages of high achievable junction temperature, higher switching speeds, and lower on-resistance as compared to the conventional silicon-based devices. In [15] and [20], GaN FETs have been utilized in distributed PV systems and show superior performance. Taking advantage of the characteristics, GaN FETs are utilized to develop high-efficient prototype converters for the proposed configuration for high efficiency and reduced size.

II. Proposed Structure

In the proposed configuration, the outputs of the subMICs are internally connected in parallel within the hosting PV module, as shown in Fig. 1(b). Each PV submodule is connected to the dedicated subMIC for MPPT. The adjacent PV modules are connected in series to build the dc-link voltage $V_{\rm DC}$. The electrical diagram of the subMICs connected within one PV module is shown in Fig. 2. The output voltage of the converters is denoted by $V_{o,x}$, where x represents the index of the PV module. The PV side components and variables are denoted by subscript "*pv,*" while output side is denoted by subscript "*o.*" The first subscript after comma represents PV module index and second subscript denotes the index of submodule.

III. Design and Analysis

Detailed analysis is carried out to investigate the mismatch handling capability of the proposed architecture. First, an iterative process is proposed for optimal design of the system as shown in Fig. 3. The number of PV modules $N_{\rm mod}$ is determined first, which is based on the minimum desired system power $P_{{\rm sys},d}$, as given in (1). The value $N_{\rm mod}$ is a rounded integer. The variable $P_{\rm mpp}$ represents the rated power of each submodule

$$N_{\rm mod} = {\rm round}\left(\frac{P_{{\rm sys},d}}{3 \times P_{\rm mpp}}\right). \tag{1}$$

The conversion ratio (*CR*) of the synchronous boost converter impacts its efficiency. Higher *CR* also results in high stress on the converter switches. Therefore, it is essential to limit the *CR* to a certain level, $CR_{\rm max}$. In ideal atmospheric conditions, all converters output the same voltage determined by $N_{\rm mod}$ and rated dc-link voltage $V_{\rm DC}$, as shown in (2). The *CR* of the boost converter is calculated in (3) and compared with the maximum value $CR_{\rm max}$, where $V_{\rm mpp,stc}$ is the MPP voltage of the submodule at STC. If the condition of $CR < CR_{\rm max}$ is satisfied, $N_{\rm mod}$ is considered as final. Otherwise, as shown in Fig. 3, the value $N_{\rm mod}$ is incremented and the process is repeated until the condition is satisfied. Moreover, the mismatch handling capability of the proposed structure and the output voltage distribution among subMICs is determined, as is illustrated in the flowchart of Fig. 4

$$V_o = \frac{V_{\rm DC}}{N_{\rm mod}} \tag{2}$$

$$\mathrm{CR} = \frac{V_o}{V_{\rm mpp,stc}}. \tag{3}$$

The multicrystalline PV cell, Qcell Q6LPT3-G2, is used as an example for the following analysis. Following the product datasheet, the photon current $I_{\rm ph}(E,T)$ and open-circuit voltage of a PV cell $V_{\rm OC}(E,T)$ in response to the variation of irradiance *E* and temperature *T* can be calculated in (4) and (5), [21], [22]. The saturation current $I_s(E,T)$ can be calculated using these values as shown in (6), where *a* is the diode ideality factor, *k* is the Boltzmann's constant and *q* is the electrical charge. The parameters α_T, β_T, and γ_E are PV cell current temperature coefficient (%/K), PV cell voltage temperature coefficient (%/K), and PV cell voltage irradiance coefficient (V·m^2/W), respectively. Finally, the MPP voltage $V_{\rm MPP}(E,T)$ and current $I_{\rm MPP}(E,T)$ of each submodule can be calculated in (7) and (8),

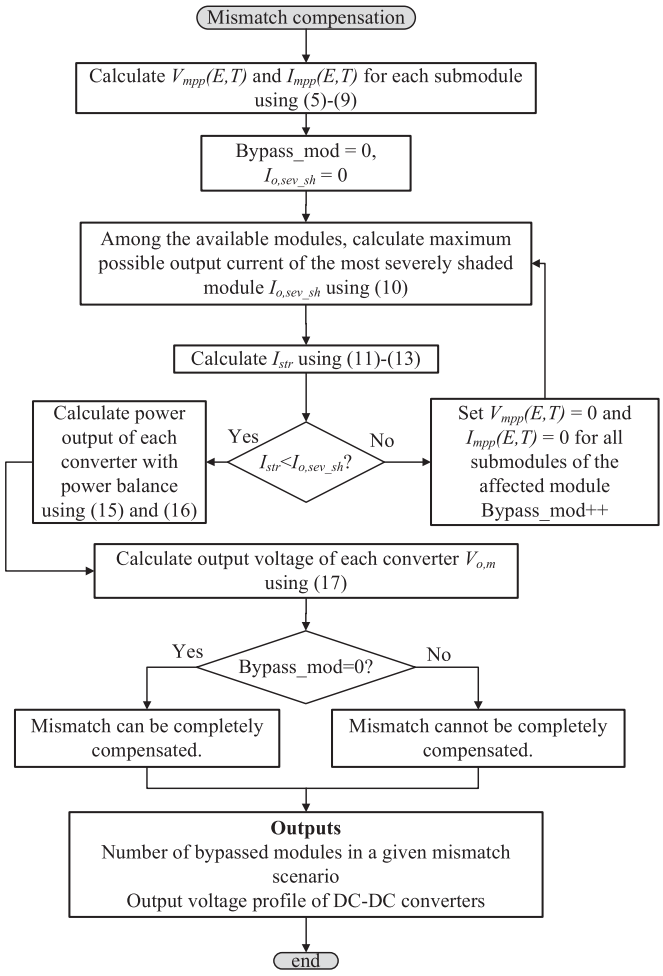

Fig. 4. Flowchart to analyze the mismatch handling capability of the proposed architecture and determine output voltage profile of dc–dc converters.

respectively

$$I_{\rm ph}\,(E,T) = \frac{E}{E_{\rm STC}} I_{\rm SCS}(1+\alpha_T \Delta T) \tag{4}$$

$$V_{\rm OC}(E,T) = V_{\rm OCS}(1+\beta_T \Delta T)(1+\gamma_E \Delta E) \tag{5}$$

$$I_s(E,T) = \frac{I_{\rm ph}(E,T)}{e^{\left[\frac{qV_{\rm OC}(E,T)}{ak(T_{\rm CS}+\Delta T)}-1\right]}} \tag{6}$$

$$V_{\rm MPP}(E,T) = N_C V_{{\rm MPP}c}(1+\beta_T \Delta T)(1+\gamma_E \Delta E) \tag{7}$$

$$I_{\rm MPP}\,(E,T) = I_{\rm ph}\,(E,T) - I_s(E,T)[e^{\frac{qV_{\rm MPP}(E,T)}{kaT_cN_c}} - 1]. \tag{8}$$

The string current I_o is the sum of the output current of three subMICs connected within one PV panel, as given in the following equation:

$$I_o = i_{o,x1} + i_{o,x2} + i_{o,x3}. \tag{9}$$

The output voltage of the three subMICs connected to a single PV panel is identical because of the parallel connection at the output terminals. Any unbalanced generation is reflected by the output current of the corresponding subMIC. On the string level, the converters form a series connection from panel to panel. So, the string current is same and the output voltages of converters connected to different PV modules reflect the changes in power produced from different PV modules.

The string current I_o is limited by the sum of the MPP currents of the converters connected to the most severely affected module (denoted by subscript *M*), as given in the following equation:

$$I_{\rm o,sev\_sh} = I_{\rm mpp,M1}(E,T) + I_{\rm mpp,M2}(E,T) + I_{\rm mpp,M3}(E,T). \tag{10}$$

The dc power $P_{\rm DC}$ available at the input of the inverter is given by (11). The output power of each subMIC is equal to the MPP power multiplied by the converter efficiency η_c as shown in (12) while the current I_o in steady state is determined as (13). The mismatch can be completely compensated only if the condition of (14) is satisfied

$$P_{\rm DC} = \sum_{k=1}^{N\rm sub} p^k_{o,\rm subMIC} \tag{11}$$

$$p^k_{o,\rm subMIC} = \eta_c V^k_{\rm mpp}(E,T) I^k_{\rm mpp}(E,T) \tag{12}$$

$$I_o = \frac{P_{\rm DC}}{V_{\rm DC}} \tag{13}$$

$$I_o < I_{o,\rm sev\_sh}. \tag{14}$$

The failed condition of (14) means that the corresponding module is needed to be bypassed. This is because a boost converter cannot step up the current and the sum of MPP currents of submodules of the affected module are less than the string current. Bypassing the affected module guarantees that while the PV module is delivering power through converters the output voltage of the converters is always higher than the input voltage. After the module is bypassed, the current in (10) is calculated using the subsequent most affected module and (11)–(14) are evaluated. The process continues till (14) is satisfied, as illustrated in the flowchart of Fig. 4. The module output power is the sum of powers of three submodules, as shown in the following equation:

$$P_{o,m} = P_{{\rm mpp},m1} + P_{{\rm mpp},m2} + P_{{\rm mpp},m3}. \tag{15}$$

Since the current at the output terminal of each PV module is constant at the value of string current I_o, the output voltage of each subMIC, denoted as $V_{o,m}$, is given in (16). It should be observed that voltage at the output of each converter is higher than the input voltage since the output current of individual subMIC is smaller than the input current

$$V_{o,m} = \frac{P_{o,m}}{I_o}. \tag{16}$$

It is pertinent to note that since the MPP currents of individual submodules add up to deliver the string current the mismatch can also be compensated for large intensity partial shading. So, if one submodule is very severely affected (because of damage, chimney shading, etc.) the remaining two submodules can cover up to provide the string current. When one submodule of a PV panel is severely shaded, its MPP current decreases decreasing the output power of the entire PV panel. This results in the decrease in output voltage of the converters since string current is constant. To follow this reduction in output voltage, the

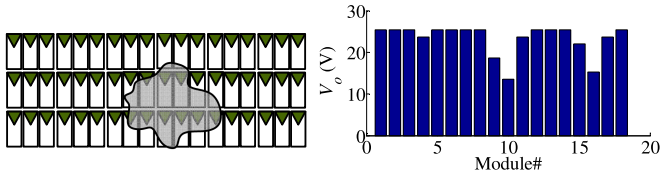

Fig. 5. (Left) Small-scale PV power system under partial shading, (right) output voltage profile of the designed system.

converters connected to healthy submodules decrease their duty cycle according to keep operating at their respective MPPs, which increases their output current. Therefore, the required string current can be compensated and achieved by healthy submodules despite the decrease in the current of one submodule. This inherent characteristic of the proposed architecture enables easier control.

A small-scale real-world system is designed and analyzed using the methods presented in this section to provide an insight into the behavior of the proposed architecture. The desired plant specifications are as follow: $P_{\mathrm{sys},d} = 5\,\mathrm{kW}$, $V_{\mathrm{DC}} = 420\,\mathrm{V}$, and $CR = 2$. The design process of Fig. 3 results in N_{mod} of 18 and P_{sys} of 5.18 kW. The PV panels are arranged into three rows each containing six panels, as shown in Fig. 5. Partial shading occurs as follow. Modules #10 and #16 are most severely shaded meanwhile two submodules in modules #9 and #15 are also partially shaded. One submodule in modules #4, #11, and #17 are affected. All other submodules in the system are unaffected and receive the highest irradiance.

The analysis method shown in Fig. 4 is applied to determine the string current and output voltage profile of converters under the predefined shading conditions. The terminal output voltage of all PV modules is illustrated in Fig. 5, which is the subMIC output within the PV modules. When all submodules receive the uniform irradiance and temperature, the output voltage of all converters should be equal to 23.3 V, according to (3). However, the output voltages of converters vary because of the inhomogeneous irradiance across the system. The converters corresponding to shaded modules decrease their output voltage; meanwhile, the converters connected to unshaded modules increase their output voltage to maintain the dc-link voltage. The output voltages of the subMICs that are connected to shaded modules are as follow: $V_{o,4} = 23.7\,\mathrm{V}$, $V_{o,9} = 18.62\,\mathrm{V}$, $V_{o,10} = 13.5\,\mathrm{V}$, $V_{o,11} = 23.7\,\mathrm{V}$, $V_{o,15} = 22\,\mathrm{V}$, $V_{o,16} = 15.2\,\mathrm{V}$, and $V_{o,17} = 23.7\,\mathrm{V}$. The converters connected to unshaded modules increase their output voltage to 25.4 V to compensate for the decrease in output voltage of converters connected to affected modules. The string current I_o is maintained as 11.1 A. The coordination can be automatically achieved by the MPPT.

IV. Modeling and Control

The primary task of the subMICs is to perform MPPT. The PV submodule voltage (v_{pv}) is selected as the MPP indicator because of its several advantages, as discussed in [23]. The control structure for individual subMIC using v_{pv} as control variable is shown in Fig. 6. The MPPT operation determines

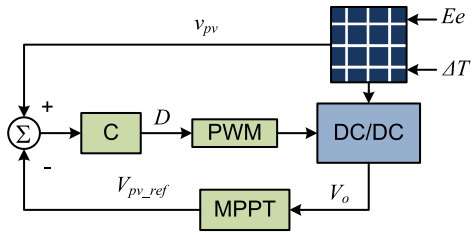

Fig. 6. Control structure of an integrated submodule and dc–dc converter.

the voltage to represent MPP. The voltage loop is regulated to follow the optimal reference.

A. Modeling

Using the techniques of averaging and linearization [21], the small-signal model is developed, as given in (17). The symbol R_L is the equivalent series resistance of inductor and the variable r_{pv}, known as dynamic resistance. The rest of the variables and parameters refer to the symbols shown in Fig. 2. The overhead cap depicts the incremental change in the variable. Since each combination of submodule and dc–dc converter is identical, the indexes of module and submodule are dropped from the symbols for simplicity

$$\frac{d}{dt}\begin{bmatrix}\hat{i}_L\\ \hat{v}_{\mathrm{pv}}\end{bmatrix}=\begin{bmatrix}-\dfrac{R_L}{L} & \dfrac{1}{L}\\ -\dfrac{1}{C_{\mathrm{pv}}} & \dfrac{1}{r_{\mathrm{pv}}C_{\mathrm{pv}}}\end{bmatrix}\begin{bmatrix}\hat{i}_L\\ \hat{v}_{\mathrm{pv}}\end{bmatrix}+\begin{bmatrix}V_o\\ 0\end{bmatrix}\hat{d}, y=\begin{bmatrix}0 & 1\end{bmatrix}\begin{bmatrix}\hat{i}_L\\ \hat{v}_{\mathrm{pv}}\end{bmatrix}. \tag{17}$$

B. Closed-Loop Controller Design

Using the state-space model of (17), the small-signal transfer function of the PV submodule voltage to duty cycle can be derived in (18) where the parameters K_o, ω_o, and ζ_o are defined in (19)

$$\frac{\hat{v}_{\mathrm{pv}}(s)}{\hat{d}(s)} = \frac{K_o}{s^2 + 2\zeta_o\omega_o s + \omega_o^2} \tag{18}$$

$$K_o = -\frac{V_o}{LC_{\mathrm{pv}}}, \omega_o = \sqrt{\frac{r_{\mathrm{pv}} - R_L}{r_{\mathrm{pv}}LC_{\mathrm{pv}}}}, \zeta_o = \frac{1}{2}\frac{r_{\mathrm{pv}}R_LC_{\mathrm{pv}} - L}{r_{\mathrm{pv}}LC_{\mathrm{pv}}\omega_o} \tag{19}$$

Using affine parameterization, the closed-loop controller for voltage regulation is derived as

$$C(s) = \frac{s^2 + 2\zeta_o\omega_o s + \omega_o^2}{K_o(\alpha_2 s^2 + \alpha_1 s)}. \tag{20}$$

C. MPPT

One of the advantages of the proposed structure is that a single microcontroller is sufficient to coordinate and regulate all subMICs within one PV panel since they share the common ground, as shown in Fig. 2. The flowchart of the MPPT algorithm is shown in Fig. 7. The index of module is dropped for simplicity while submodules indices are shown. The perturb and observe algorithm is implemented to track MPP of each

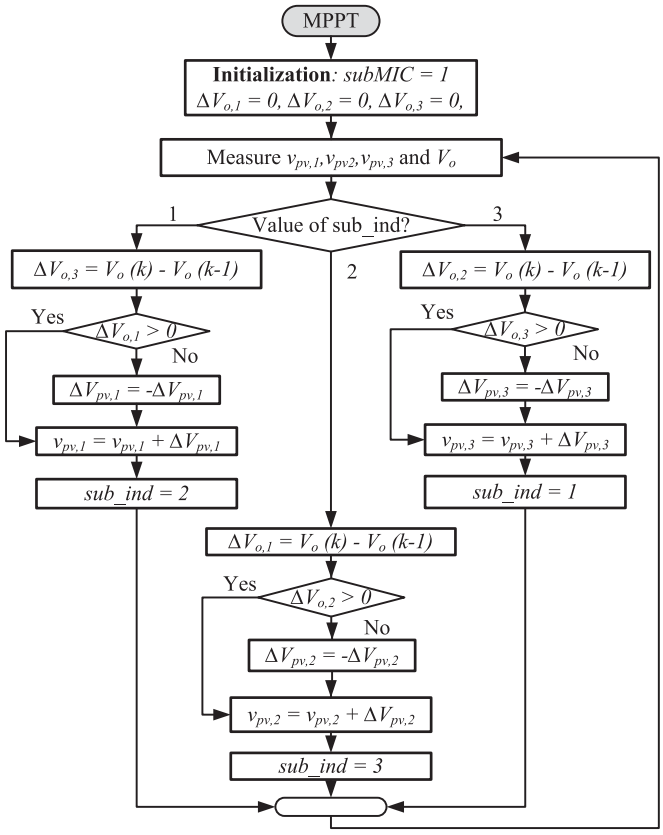

Fig. 7. Flowchart of the unified MPPT algorithm for the three subMICs connected to submodules of a single PV panel.

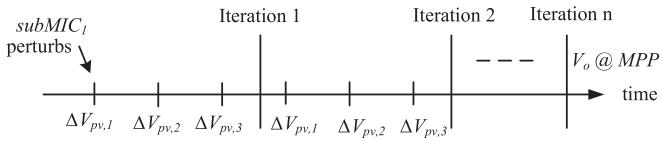

Fig. 8. Timeline of the unified MPPT algorithm for the three subMICs connected to submodules of a single PV panel.

submodule. The measurements include voltages of submodules $v_{\mathrm{pv},1}$, $v_{\mathrm{pv},2}$, $v_{\mathrm{pv},3}$ and output voltage V_o, which is identical for three subMICs.

Since the current I_o can be considered constant for each MPPT cycle, V_o is used as the power indicator. In Fig. 7, the variables $\Delta V_{o,1}$, $\Delta V_{o,2}$ and $\Delta V_{o,3}$ signify the change in output voltage due to perturbation in $v_{\mathrm{pv},1}$, $v_{\mathrm{pv},2}$, and $v_{\mathrm{pv},3}$, respectively. The perturbations are sequentially applied to avoid any conflict among subMICs, which is demonstrated by the timeline of the algorithm provided in Fig. 8. The variable *sub_ind* holds the index of the active subMIC being controlled. The direction of tracking for each subMIC is decided by observing the change in V_o caused by the perturbation in PV voltage of the respective submodule. If the change in V_o is negative, the direction of tracking is reversed, otherwise, the tracking continues in the same direction.

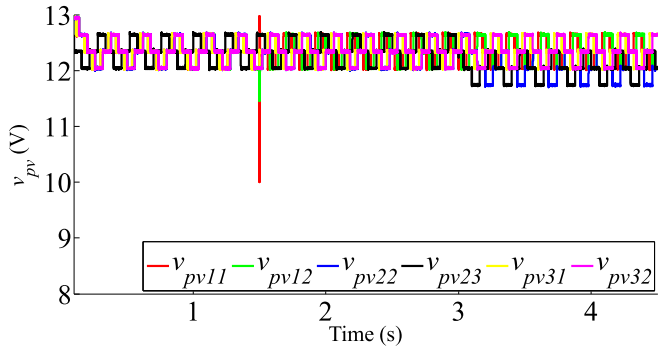

Fig. 9. PV submodule voltages.

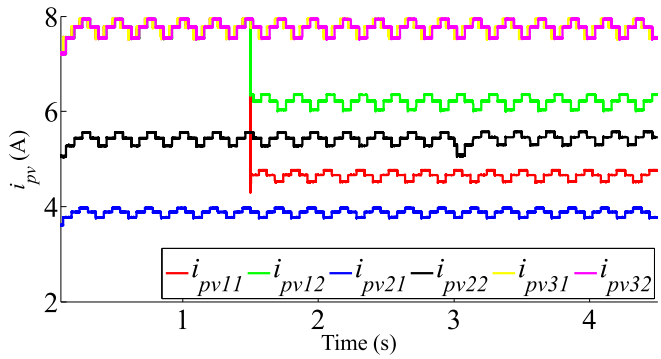

Fig. 10. PV submodule currents.

V. Simulation and Concept Proof

To prove the concept, a scaled-down system consisting of 12 submodules and 12 subMICs is simulated to investigate the system response under variations of *E* and T. The test scenario is explained as follow. The submodules SM_{11} and SM_{12} suffer *E* change at $t = 1.5$ s from 1 to 0.6 and 0.8 kW/m^2, respectively, while SM_{21} and SM_{22} receive a reduced *E* of 0.7 and 0.5 kW/m^2, respectively. The rest of the submodules in the system receive a uniform irradiance of 1 kW/m^2. The variation in *T* occurs at $t = 3$ s where SM_{22} and SM_{23} experience a temperature change of from 25 °C to 30 °C and 25 °C to 33 °C, respectively. All the other submodules in the system receive a constant *T* of 25 °C.

Figs. 9 and 10, respectively, illustrate the behavior of voltages and currents of the affected submodules. It can be observed from Fig. 9 that there is a momentary dip shown in voltages $v_{\mathrm{pv}11}$ and $v_{\mathrm{pv}12}$ since the corresponding submodules are experiencing a transition to lower irradiance. The condition results from the operating point entering the saturation region of current–voltage (*I–V*) curve to output high current to match string current. The MPPT controller takes action and adjusts duty cycle corresponding to the reference PV voltage value in the fast voltage regulation loop. The condition results from the operating point entering the saturation region of current–voltage (*I–V*) curve to output high current to match string current. At $t = 3$ s voltages $v_{\mathrm{pv}21}$ and $v_{\mathrm{pv}22}$ change in response to temperature gradients. The currents $i_{\mathrm{pv}12}$ and $i_{\mathrm{pv}12}$ decrease at $t = 1.5$ s as irradiance is decreased while the currents $i_{\mathrm{pv}21}$ and $i_{\mathrm{pv}22}$ remain the same

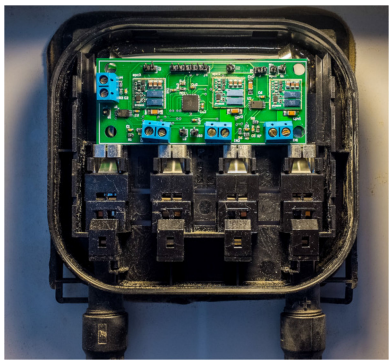

Fig. 11. Junction box of a PV panel (Schott-240 W) is implemented with three subMICs including six GaN FETs.

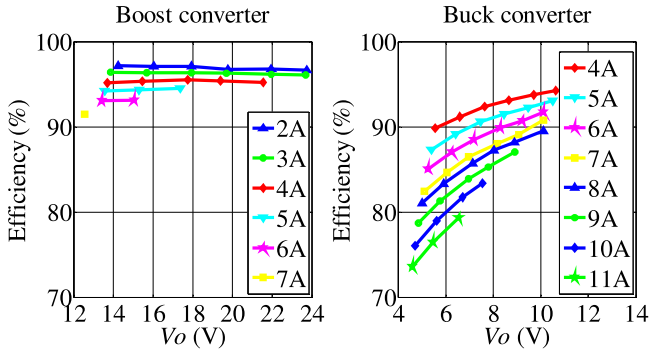

Fig. 12. Experimental efficiency curves of the benchmark system (buck) and proposed system (boost) for a range of string currents.

TABLE I
COMPONENT LIST PER JUNCTION BOX

Device	Model	Synchronous Buck		Synchronous Boost	
		Quantity	Cost	Quantity	Cost
GaN Switches	EPC2021	6	7.44	6	7.44
FET Driver	LM5113	3	2.29	3	2.29
Inductor	SER103KL (10 μH)	3	0.92	3	0.92
Input cap	25 V/4.7 μF	-	-	3	0.044
	25 V/10 μF	6	0.075	-	-
Output cap	10 μF	3	0.10	3	0.228
Microcontroller	dsPIC33FJ16GS502	3	3.60	1	3.60
OpAmp	MCP6022	2	0.99	1	0.99
Total cost (US$)		67.8		59.7	

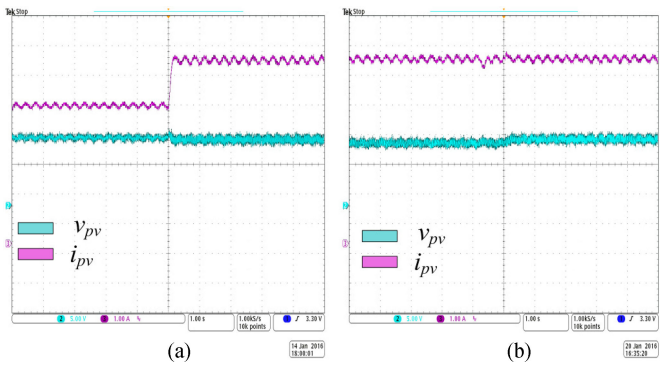

Fig. 13. Experimental results of MPPT operation in response to the (a) E variation from 0.6 to 0.8 kW/m^2 (b) T changes from 30 °C to 25 °C.

through the test duration as submodules SM_{21} and SM_{22} are constantly under shade. It can be observed from Figs. 9 and 10 that the voltages ($v_{\mathrm{pv}31}$, $v_{\mathrm{pv}32}$) and currents ($i_{\mathrm{pv}31}$, $i_{\mathrm{pv}32}$), which represent healthy submodules do not experience any change in operation point thus validating independent MPPT operation of each subMIC in the system. The new MPP of each submodule is quickly reached after any transient variation.

VI. Experimental Evaluation

Both subMIC systems, as shown in Fig. 1, are evaluated experimentally to compare the performance in terms of efficiency, system dynamics, and cost. Since three subMICs are required to fit into one PV panel, subMICs were designed and constructed using GaN FETs at 250 kHz to meet the requirement. The prototyped synchronous boost-based subMICs are shown in Fig. 11, which shows the converters fit in the junction box of the PV panel, model #Schott-240 W. For a fair comparison of the proposed solution and the benchmark, a synchronous buck converter is also constructed using the comparable specifications. Both converters are rated in accordance to a 100-W submodule with input voltage of 15 V. The proposed solution meets the voltage ripple requirement using a smaller input capacitance (4.7 μF) as compared to the benchmark (20 μF). The costs of the hardware prototypes of both subMIC are compared side by side, as listed in Table I. The total cost is calculated for three subMICs needed for individual PV panel. The proposed solution shows 14% lower cost than the benchmark system since the advanced structure allows using one microcontroller and one op-amp to achieve the required control, MPPT, and sensing task. Agilent solar array simulator E4350B is used to emulate the PV submodule, while an electronic load is used to realize the constant string current.

Fig. 12 shows the efficiency comparison between the benchmark system and the proposed system. The benchmark shows lower efficiency ranging from 80% to 90% based on different power profile. The proposed system shows the advantage in efficiency, which range from 93% to 97% for the tested operation conditions. Fig. 13(a) illustrates the MPPT operation when irradiation changes from 0.6 to 0.8 kW/m^2, while the temperature is maintained at 25 °C. The variation of v_{pv} and i_{pv} can be noticed in the experimental results of Fig. 13(b) when the temperature changes from 30 to 25 °C, while the constant irradiance of 1 kW/m^2 is maintained.

VII. Conclusion

This paper presented a novel PV system architecture for submodule-level MPPT implementation. The subMIC prototype employs Gallium Nitride (GaN) power switches, which allow high conversion efficiency and reduction in size.

The step-by-step theoretical analysis and computer-aided design lead to the full system sizing and development. The synchronous boost converter is utilized as the subMIC interface

owing to the proven fast dynamic response and low cost implementation. The system effectiveness in terms of configuration and control is examined by the simulation of various atmospheric conditions in terms of irradiance and temperature. The hardware prototypes are designed and constructed, which include a benchmark system that is based on the conventional subMIC system. The proposed architecture demonstrates the advantage of simplicity, low-cost, efficiency improvement, and fast dynamics superior than the conventional subMIC approach.

REFERENCES

[1] S. B. Kjaer, J. K. Pedersen, and F. Blaabjerg, "A review of single-phase grid-connected inverters for photovoltaic modules," *IEEE Trans. Ind. Appl.*, vol. 41, no. 5, pp. 1292–1306, Sep./Oct. 2005.

[2] S. Strache, R. Wunderlich, and S. Heinen, "A comprehensive, quantitative comparison of inverter architectures for various PV systems, PV cells, and irradiance profiles," *IEEE Trans. Sustain. Energy*, vol. 5, no. 3, pp. 813–822, Jul. 2014.

[3] A. Maki and S. Valkealahti, "Power losses in long string and parallel-connected short strings of series-connected silicon-based photovoltaic modules due to partial shading conditions," *IEEE Trans. Energy Convers.*, vol. 27, no. 1, pp. 173–183, Mar. 2012.

[4] C. Huang-Jen *et al.*, "A module-integrated isolated solar microinverter," *IEEE Trans. Ind. Electron.*, vol. 60, no. 2, pp. 781–788, Feb. 2013.

[5] S. Ben-Yaakov, A. Blumenfeld, A. Cervera, and M. Evzelman, "Design and evaluation of a modular resonant switched capacitors equalizer for PV panels," in *Proc. 2012 IEEE Energy Convers. Congr. Expo.*, 2012, pp. 4129–4136.

[6] A. Blumenfeld, A. Cervera, and M. M. Peretz, "Enhanced differential power processor for PV systems: Resonant switched-capacitor gyrator converter with local MPPT," *IEEE J. Emerg. Sel. Topics Power Electron.*, vol. 2, no. 4, pp. 883–892, Dec. 2014.

[7] P. S. Shenoy, K. A. Kim, B. B. Johnson, and P. T. Krein, "Differential power processing for increased energy production and reliability of photovoltaic systems," *IEEE Trans. Power Electron.*, vol. 28, no. 6, pp. 2968–2979, Jun. 2013.

[8] C. Olalla, C. Deline, and D. Maksimovic, "Performance of mismatched PV systems with submodule integrated converters," *IEEE J. Photovolt.*, vol. 4, no. 1, pp. 396–404, Jan. 2014.

[9] Q. Shibin, S. T. Cady, A. D. Dominguez-Garcia, and R. C. N. Pilawa-Podgurski, "A distributed approach to maximum power point tracking for photovoltaic submodule differential power processing," *IEEE Trans. Power Electron.*, vol. 30, no. 4, pp. 2024–2040, Apr. 2015.

[10] J. T. Stauth, M. D. Seeman, and K. Kesarwani, "Resonant switched-capacitor converters for sub-module distributed photovoltaic power management," *IEEE Trans. Power Electron.*, vol. 28, no. 3, pp. 1189–1198, Mar. 2013.

[11] N. Femia, G. Lisi, G. Petrone, G. Spagnuolo, and M. Vitelli, "Distributed maximum power point tracking of photovoltaic arrays: Novel approach and system analysis," *IEEE Trans. Ind. Electron.*, vol. 55, no. 7, pp. 2610–2621, Jul. 2008.

[12] G. R. Walker and P. C. Sernia, "Cascaded DC-DC converter connection of photovoltaic modules," *IEEE Trans. Power Electron.*, vol. 19, no. 4, pp. 1130–1139, Jul. 2004.

[13] R. C. N. Pilawa-Podgurski and D. J. Perreault, "Submodule integrated distributed maximum power point tracking for solar photovoltaic applications," *IEEE Trans. Power Electron.*, vol. 28, no. 6, pp. 2957–2967, Jun. 2013.

[14] F. Wang, X. Wu, F. C. Lee, and F. Zhuo, "Analysis of unified output MPPT control in sub-panel PV converter system," *IEEE Trans. Power Electron.*, vol. 29, no. 3, pp. 1275–1284, Mar. 2014.

[15] O. Khan, W. Xiao, and H. H. Zeineldin, "Gallium nitride based submodule integrated converters for high-efficiency distributed maximum power point tracking PV applications," *IEEE Trans. Ind. Electron.*, vol. 63, no. 2, pp. 966–975, Feb. 2016.

[16] O. Khan and W. Xiao, "An efficient modeling technique to simulate and control submodule-integrated PV system for single-phase grid connection," *IEEE Trans. Sustain. Energy*, vol. 7, no. 1, pp. 96–107, Jan. 2016.

[17] W. Xiao, N. Ozog, and W. G. Dunford, "Topology study of photovoltaic interface for maximum power point tracking," *IEEE Trans. Ind. Electron.*, vol. 54, no. 3, pp. 1696–1704, Jun. 2007.

[18] B. J. Baliga, *Power Semiconductor Devices (General Engineering)*, 1st ed. Boston, MA, USA: PWS, 1995.

[19] F. C. Lee and L. Qiang, "High-frequency integrated point-of-load converters: Overview," *IEEE Trans. Power Electron.*, vol. 28, no. 9, pp. 4127–4136, Sep. 2013.

[20] M. Kasper, D. Bortis, and J. W. Kolar, "Classification and comparative evaluation of PV panel-integrated DC-DC converter concepts," *IEEE Trans. Power Electron.*, vol. 29, no. 5, pp. 2511–2526, May 2014.

[21] W. Xiao, F. F. Edwin, G. Spagnuolo, and J. Jatskevich, "Efficient approaches for modeling and simulating photovoltaic power systems," *IEEE J. Photovolt.*, vol. 3, no. 1, pp. 500–508, Jan. 2013.

[22] O. Khan and W. Xiao, "An efficient modeling technique to simulate and control submodule-integrated PV system for single-phase grid connection," *IEEE Trans. Sustain. Energy*, vol. 7, no. 1, pp. 96–107, Jan. 2016.

[23] W. Xiao, W. G. Dunford, P. R. Palmer, and A. Capel, "Regulation of photovoltaic voltage," *IEEE Trans. Ind. Electron.*, vol. 54, no. 3, pp. 1365–1374, Jun. 2007.